Observations of gravel beach dynamics during high energy wave conditions using a laser scanner

L.P. Almeida, G. Masselink, P.E. Russell, M.A. Davidson

Corresponding author email: luis.melodealmeida@plymouth.ac.uk; or melolp@gmail.com

PII: S0169-555X(14)00427-9
DOI: 10.1016/j.geomorph.2014.08.019

Please cite this article as: Almeida, L.P., Masselink, G., Russell, P., Davidson, M., Observations of gravel beach dynamics during high energy wave conditions using a laser scanner, *Geomorphology* (2014), doi: 10.1016/j.geomorph.2014.08.019

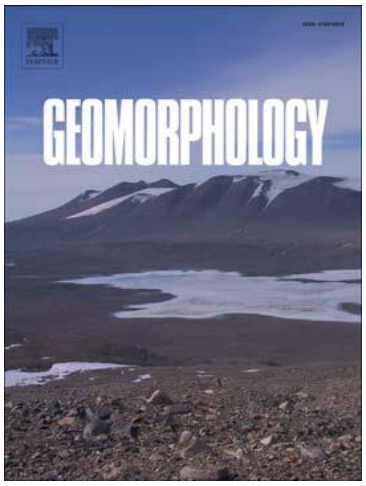

Abstract

A 2D laser-scanner was deployed at the high tide runup limit of a pure gravel beach (Loe Bar, Cornwall, England) to measure high-frequency (2.5 Hz) swash hydrodynamics and topographic changes during an energetic wave event. Measurements performed with the laser-scanner were corrected to compensate for levelling and orientation errors, and a variance threshold was applied to separate the beach topography from the water motions. Laser measurements were used to characterise the swash hydrodynamics and morphological changes during one tidal cycle through the calculation of several parameters, such as the 2% exceedence of the runup maxima ($R_{2\%}$), swash flow velocity skewness ($< u^3 >$), runup spectra and cumulative topographic changes. Results indicate that despite the small net morphological changes over the tide cycle, significant sediment mobilization occurs. A clear asymmetrical morphological response was found during the different tidal phases: the rising tide is dominated by accretion whilst the falling tide is dominated by erosion. The main factor controlling this asymmetrical morphological response is the step migration that, depending on the tide phase, controls the wave breaking point and consequently the dominant sediment transport direction. During the rising tide, step development decreases the shoreface slope and reduces the runup energy, whilst during the falling tide the step remobilization increases the shoreface slope and energy on the runup.

Keywords

Swash zone; Remote sensing; Bed evolution; Hydrodynamics; Gravel beaches

1. Introduction

Gravel beaches and barriers occur typically along paraglacial coasts (e.g., Canada, UK, Ireland) or coastlines backed by mountains (e.g., Mediterranean, New Zealand), and according to Jennings and Schulmeister (2002) they can be found in nature mainly in three different forms: (1) pure gravel beach; (2) mixed sand and gravel; and (3) composite gravel beach. Pure gravel beaches (hereafter referred as 'gravel beach') are characterised by steep reflective profiles and prominent secondary morphological features, such as ridges, berms, step and cups, but without nearshore bars (Buscombe and Masselink, 2006). During highly energetic wave conditions (e.g., storms), gravel beaches typically dissipate most of the offshore wave energy across a narrow cross-shore section next to the swash zone (Buscombe and Masselink, 2006, Ruiz de Alegria-Arzaburu and Masselink, 2010 and Poate et al., 2013). The absence of an offshore bar promotes large collapsing/plunging waves to break on the lower beachface (step) creating extremely energetic boundary conditions for swash motions and enhancing highly turbulent flows capable of mobilizing significant amounts of gravel at individual swash time scales (Austin and Masselink, 2006, Austin and Buscombe, 2008 and Masselink et al., 2010). Under such energetic conditions, the complex interactions between the swash hydrodynamics and the beach morphology dictate the occurrence and extension of hazardous events like barrier overtopping or overwashing (Orford et al., 2003 and Matias et al., 2012). The acquisition of full-scale, hydro- and morpho-dynamic measurements is essential in order to provide new insights into the fundamental processes driving coastal change, overtopping and flooding. However, the deployment of any kind of in-situ measurements in such energetic conditions is extremely challenging. Of particular importance to the study of sediment transport in the swash zone is the development of instruments with the ability to acquire reliable measurements of both swash hydrodynamics and bed changes at wave-by-wave time scales.

Recently, a method based on ultrasonic technology brought the innovative capability to quantify bed changes and water motions at a frequency of individual uprush–backwash events with the accuracy of ± 1 mm (Turner et al., 2008). This method is typically mounted on a scaffold frame with a large number of ultrasonic units (bed-level sensors — BLS), equally spaced at a certain elevation (~ 1.5 m) from the bed, allowing the acquisition of the bed changes, swash position and volume at 4 Hz (Turner et al., 2008). The capability of this method has been very well demonstrated in several field (e.g., Masselink et al., 2009, Masselink et al., 2010, Blenkinsopp et al., 2011 and Poate et al., 2013) and laboratory (e.g., Masselink and Turner, 2012, Williams et al., 2012 and Masselink et al., 2013) applications.

A limitation of having to use a large scaffold frame for mounting the large number of sensors required to obtain data of sufficient spatial coverage is that the methodology is only possible for mild wave conditions. This logistical problem is exacerbated on gravel beaches where typically most of the offshore wave energy is dissipated over the swash zone and the breaker region just seaward of the swash zone (Buscombe and Masselink, 2006, Ruiz de Alegria-Arzaburu and Masselink, 2010 and Poate et al., 2013).

Remote sensing methods emerge in this context as the most appropriate solution for this type of field measurements, especially under energetic wave conditions that lead to the most dramatic morphological changes. During the last three decades video imaging has been the most applied remote sensing method to nearshore surveying. The estimation of intertidal topography (e.g., Plant and Holman, 1997) and nearshore bar location (e.g., Lippmann and Holman, 1989) or subtidal bathymetry (e.g., Stockdon and Holman, 2000) are all examples of the wide variety of applications that video can offer. Video data are also extensively used in runup studies and several runup parameterizations (e.g., Holman, 1986 and Stockdon et al., 2006) are based on video measurements. Despite the high spatial and temporal resolution that video runup data can offer, video imaging does present some significant limitations regarding their use during storms, such as the inability to record useful data during low light (e.g., during the night) or rainy and foggy conditions (typical conditions during storms). In addition, conversion of video data from image coordinates to real-world coordinates requires information on the beach morphology and this is not a constant during a storm.

Recent studies reporting the use of laser-scanners on natural beaches (Blenkinsopp et al., 2010, Brodie et al., 2012 and Almeida et al., 2013) and laboratories (Blenkinsopp et al., 2012) have demonstrated the ability of the laser technology to measure swash hydrodynamics, as well as bed evolution, on the swash event time scale remotely (i.e., without the need to deploy the instrument within the region of interest). The versatility and precision of 2D laser-scanners have enabled the development of a large range of useful non-contact measurement applications ranging from medicine (e.g., Pallejà et al., 2009), forestry (e.g., Miettinen et al., 2007), to robotics (e.g., Vásquez-Martín et al., 2009). Using a simple ‘time of flight’ working principle to compute the distance between the laser sensor and the ‘target’, this method allows the acquisition of high-frequency and fine spatial resolution measurements along a swath line within the laser beam range.

Comparisons between 2D laser-scanners and state-of-the-art instrumentation, such as ultrasonic altimeters, video cameras and capacitance wave probes, have showed that the accuracy of the laser is comparable to that of the standard methods (Blenkinsopp et al., 2010, Blenkinsopp et al., 2012 and Almeida et al., 2013), but these preliminary comparative efforts present limited information on important aspects of the laser technique, such as instrument deployment and data processing.

The aim of the present work is to provide guidance on how to deploy a 2D laser-scanner in the field to collect high-frequency topographic and hydrodynamic data from the swash, together with methods to process the raw laser measurements. As a demonstration of the capabilities of this instrument we also present a detailed analysis of the morphodynamics of a gravel beach (Loe Bar, UK) during an energetic tidal cycle.

2. Methods

2.1. Study site and field deployment

A field experiment was conducted between 23 February and 28 March 2012 at Loe Bar in the southwest of England (Fig. 1) with the aim of monitoring the response of a gravel beach to varying wave conditions (cf. Poate et al., 2013). Loe Bar is part of a 4.3-km long gravel beach (D_{50} = 2–4 mm) that extends from Porthleven, in the north, to Gunwalloe, in the south (Fig. 1). The Loe Bar barrier fronts Loe Pool and extends 430 m between the adjacent headlands, with an average width of 200 m and a typical seaward gradient of 0.1. With a NW–SE shoreline orientation, the barrier faces south-west and is exposed to energetic Atlantic swell with an annual average significant wave height (H_s) of 1.2 m, an average peak period (T_p) of 9.1 s and a direction (θ) of 235° (wave statistics were derived from Porthleven wave buoy measurements from October 2011 to October 2012; data can be downloaded freely from http://www.channelcoast.org). The tidal regime is macrotidal with MHWS (mean high water spring) and MLWS (mean low water spring) at, respectively, 2.5 m and − 2.2 m ODN (Ordnance Datum Newlyn; 0 m ODN ~ 0.2 m above mean sea level in UK coastal waters).

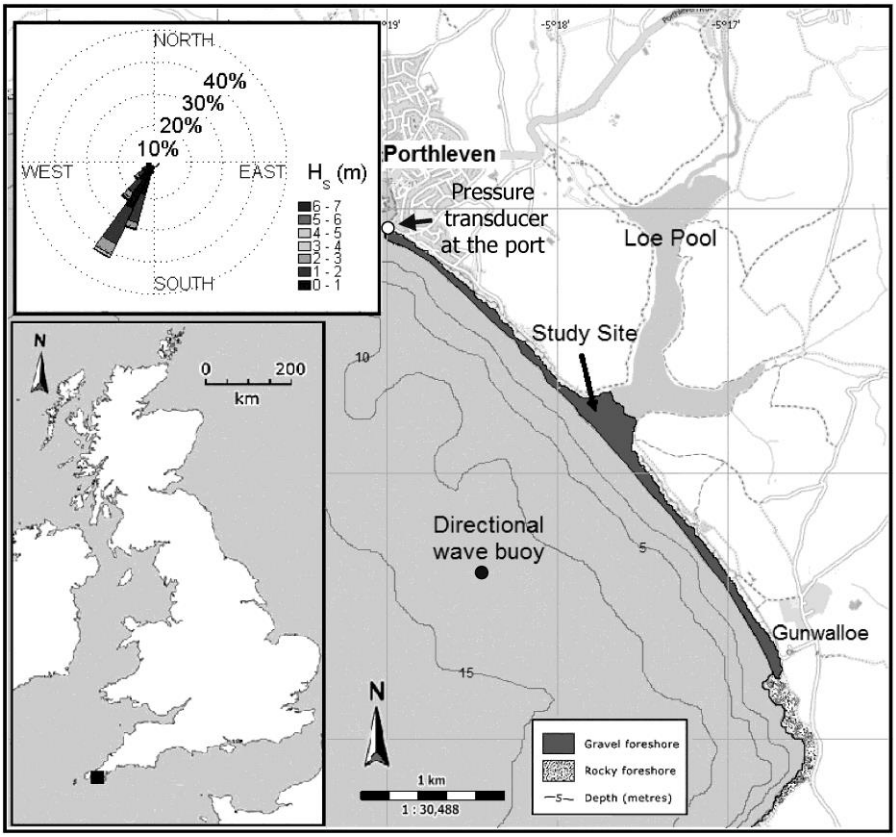

Fig. 1. Map showing the location of the study site (Loe Bar), the location of the offshore wave buoy and bathymetry. The wave rose represents 1 year (from October 2011 to October 2012) of directional wave buoy data.

A 2D laser-scanner (SICK — LD-OEM3100) was deployed on the top of an aluminium tower (5.2 m high), fixed to a scaffold frame inserted into the beach around the high tide runup level and stabilized by guy ropes (Fig. 2). External power supply (28 V) is provided to the scanner during operation and

measurements are streamed to a laptop, by an RS422 cable, where data are recorded using the SOPAS (SICK) software interface.

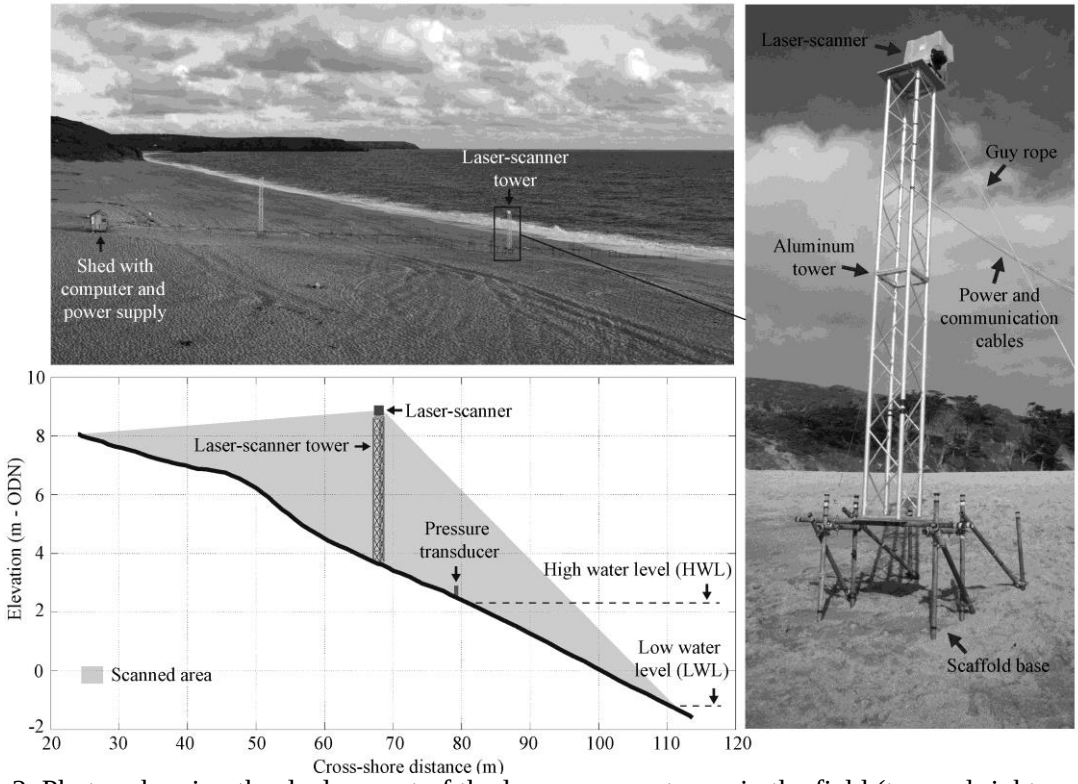

Fig. 2. Photos showing the deployment of the laser-scanner tower in the field (top and right panels). Lower left panel shows the beach profile with locations of the equipment used during the survey.

A pressure transducer was deployed just above the high water level (Fig. 2) to measure swash/wave conditions (at 4 Hz) in the lower swash zone during mid- and high-tide conditions, and offshore wave conditions were measured by a Porthleven directional wave buoy located at approximately 10 m water depth at low tide (Fig. 1). Tide measurements were performed at Porthleven port (Fig. 1) by a pressure transducer deployed around the MLWS level, and the beach topography was surveyed at each low tide along the laser-scanner profile using a dGPS (Trimble 5800).

2.2. The 2D laser-scanner and working principle

The LD-OEM3100 laser scanner model was selected for the present work. This model is a two-dimensional mid-range (maximum range ≈ 100 m; SICK, 2009) laser-scanner that emits pulsed laser beams (invisible infrared light; λ = 905 nm) that are deflected on an internal mirror (inside the scanner head) that rotates at regular angular steps and scans the surroundings (360°) in a circular manner (Fig. 3). The scanner head rotates at 2.5 Hz with an angular resolution of 0.125° and the distance to the target is calculated from the propagation time that the light requires from emission to reception of the reflection at the sensor.

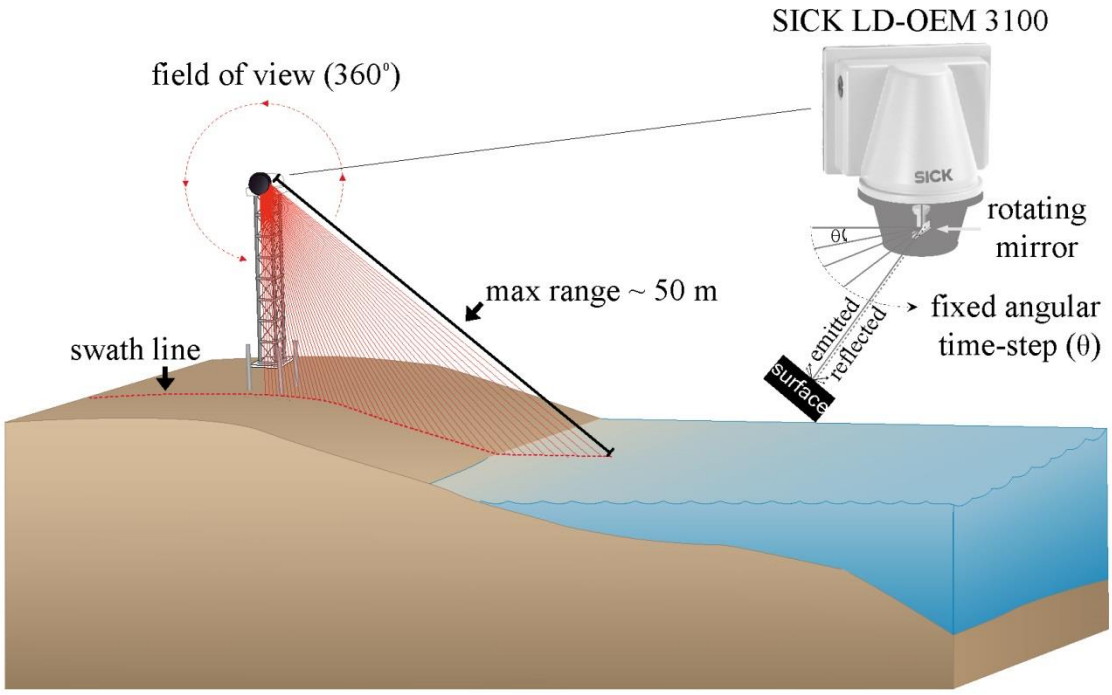

Fig. 3. Diagram of the 2D laser-scanner LD-OEM3100 (SICK) showing working principles in the field.

The measurements are logged at 2.5 Hz and consist of two dimensional polar coordinates (d_i, α_i), where i is the scan number (complete cycle of scanner field of view), d is the distance measured between the laser-scanner and the target and α is the relative angle of the measurement. The number of measurements per scan is given by the scan angle divided by the angular resolution, e.g., for a scan angle of 120°, the number of measurements is 960.

3. Results

3.1. Correction of the laser measurement position and orientation

Laser polar measurements (d_i, α_i) are initially converted to Cartesian coordinates (x_i, z_i), where x is the cross-shore position and z elevation, by applying a polar transformation. This new coordinate system is referred to a local coordinate system, where the cross-shore origin ($x = 0$) is at the top of the barrier and the vertical datum is referred to the Ordnance Datum of Newlyn (ODN).

It is extremely difficult in the field to deploy the laser tower perfectly vertical; therefore, the laser measurements are characterised by an orientation offset with respect to the ground level. A beach profile derived from the laser scanner data will therefore have inaccuracies when compared with the real profile (Fig. 4). To correct this orientation problem, the Horn's quaternion-based method for absolute orientation (Horn, 1987) is implemented. This method minimizes the sum of the squared distances between two datasets of points, and for the present purpose the laser measurements were corrected using differential GPS (dGPS) measurements (performed on the swath line of the laser) by applying the following equation:

$$\sum_{j=1}^{n} \left\| r\left(Xlaser_j, Zlaser_j\right) + t - \left(Xgps_j, Zgps_j\right) \right\|^2 \qquad (equation\ 1)$$

where r is the unknown rotation matrix (due to orientation problem) and t the unknown translation vector (position of laser coordinate system relative to that of local GPS coordinate system), $Xlaser_j$ and $Zlaser_j$ are the laser coordinates, $Xgps_j$ and $Zgps_j$ are the GPS coordinates, and $j = 1,\ldots,n$ represents the number of points.

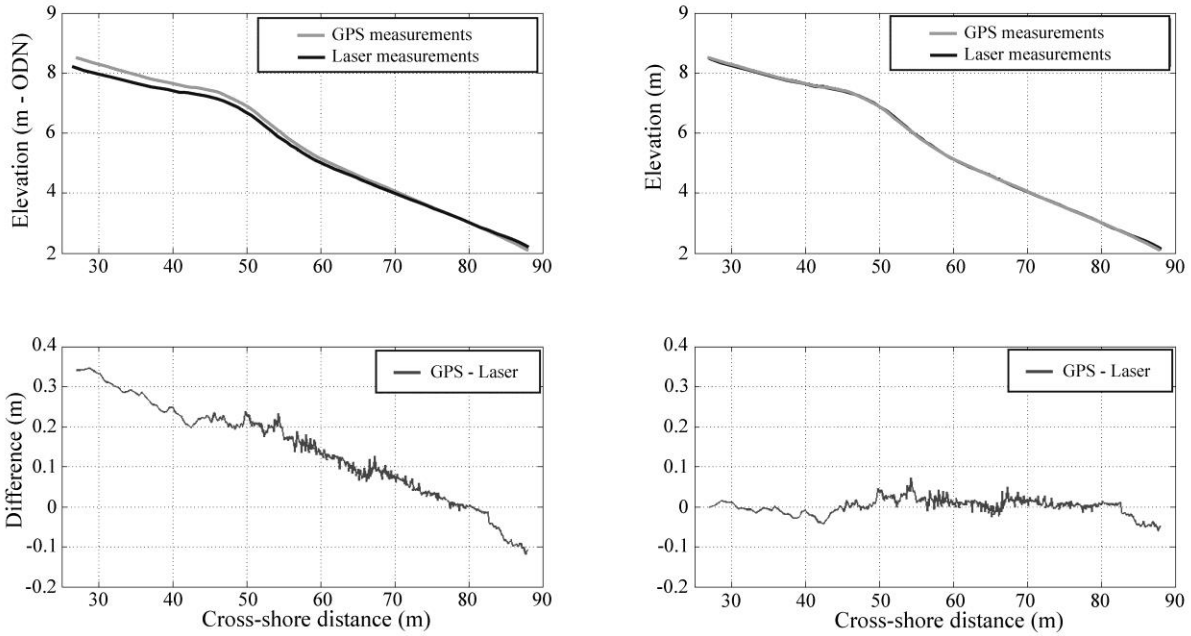

Fig. 4. Comparison between laser-derived beach morphology and that measured using dGPS. Upper panels show comparison between dGPS profile and raw laser-derived profile (upper-left panel) and between dGPS profile and laser-derived profile corrected for mis-orientation and translation (upper-right panel). The lower panels show the associated residuals (difference between dGPS profile and laser-derived profile).

As evident from Fig. 4, after applying Eq. (1) to the laser measurements, this angular offset is eliminated and the remaining residuals are within the accuracy of the dGPS (approximately ± 5 cm in vertical).

3.2. Scanning coverage and horizontal resolution

With the present deployment (5.2 m tower elevation) the laser-scanner covered approximately 90 m of a cross-section of the beach with an average horizontal resolution of 6 cm (Fig. 5). On the upper and the lower part of the profile (landward from the berm crest and lower shoreface) the horizontal resolution was lower (between 20 cm and 1 m), due to the low angle of incidence that increased significantly the space between measurements (Fig. 5). Better average horizontal resolution could be attained by lowering the laser-scanner tower (e.g., 1 m elevation — see Fig. 5), although this would reduce dramatically the number of measurements on the top of the berm and on the bottom of the shoreface, reducing the scanning coverage. By elevating the laser-scanner tower, the swath line coverage would increase, although reducing the horizontal resolution. In this case the distance would affect the angular step (e.g., with the same angular step the horizontal resolution decreases with distance) and reduce the horizontal resolution, although other problems such as the tower stability or the reduction of the power of the reflected beam (Pallejà et al., 2009) would affect the measurements with the raised tower. For all these reasons the present tower elevation and cross-shore location were found to be optimal for data collection on the swash zone of this site.

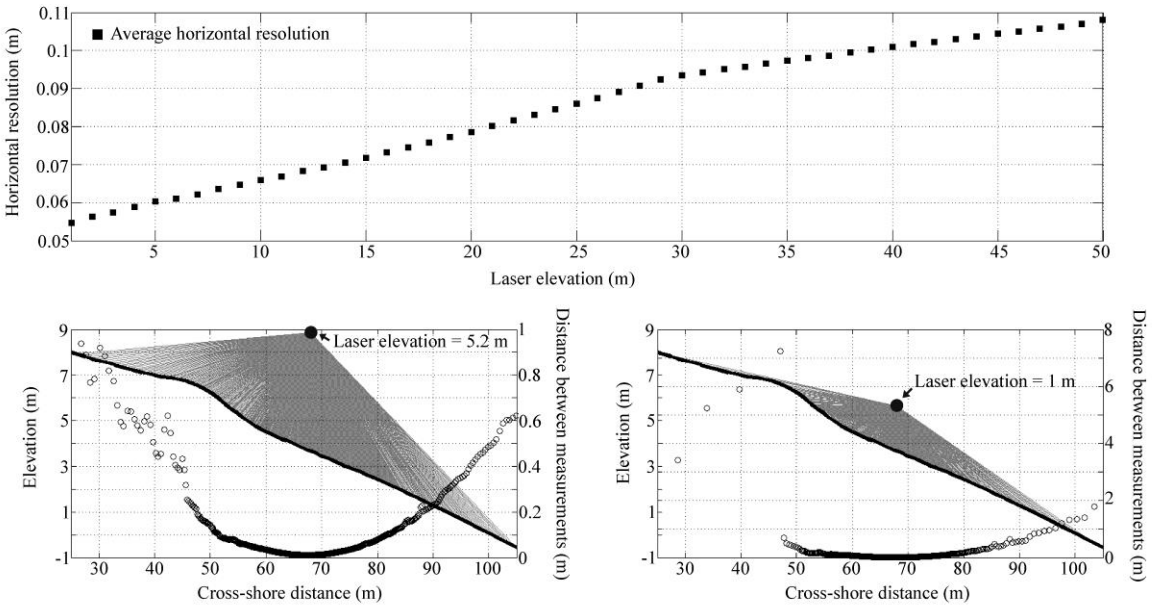

Fig. 5. Average horizontal resolution of the laser-scanner measurements computed for different tower elevations, assuming 0.125 angular resolution and the same cross-shore position (top panel). Example of the laser-scanner horizontal resolution (black dots) computed for the laser-scanner beams (grey lines) using different laser-scanner elevations (5.2 — bottom left panel and 1 m — bottom right panel).

3.3. Separation between the bed level and water surface

The raw laser measurements represent reflection of the laser beams from the beach topography as well as the water surface, without any distinction between the two (Fig. 6). To separate topography from the water at each cross-shore position, and over time, a moving-average time window with a variable variance threshold is applied to all measurements (Eq. (2)):

$$Ztopo_{(\Delta t)} = \overline{Zlaser_{(\Delta t)}} \quad if \quad \sigma^2\left(Zlaser_{(\Delta t)}\right) \leq \sigma^2_{threshold} \qquad (equation\ 2)$$

where Δt is the time window length (4 s — period of time required for the natural variance of the signal to stabilize after the passage of a wave, defined empirically) and $\sigma^2_{threshold}$ is the variance threshold (see next section). This method of separating the stationary bed level from the non-stationary water surface (wave or swash) is similar to that used by Turner et al. (2008) for data collected using ultrasonic bed-level sensors (BLS). The time-varying vertical position of the water's edge on the foreshore of the beach (runup) is then obtained by subtracting the extracted topography (*Ztopo*) from the raw measurements (*Zlaser*), and using a threshold water depth (0.02 m) to define the instantaneous shoreline. By applying this separation method, the raw laser measurements are separated into two distinct time series of topographic measurements and hydrodynamics (Fig. 6), and can then be independently analysed.

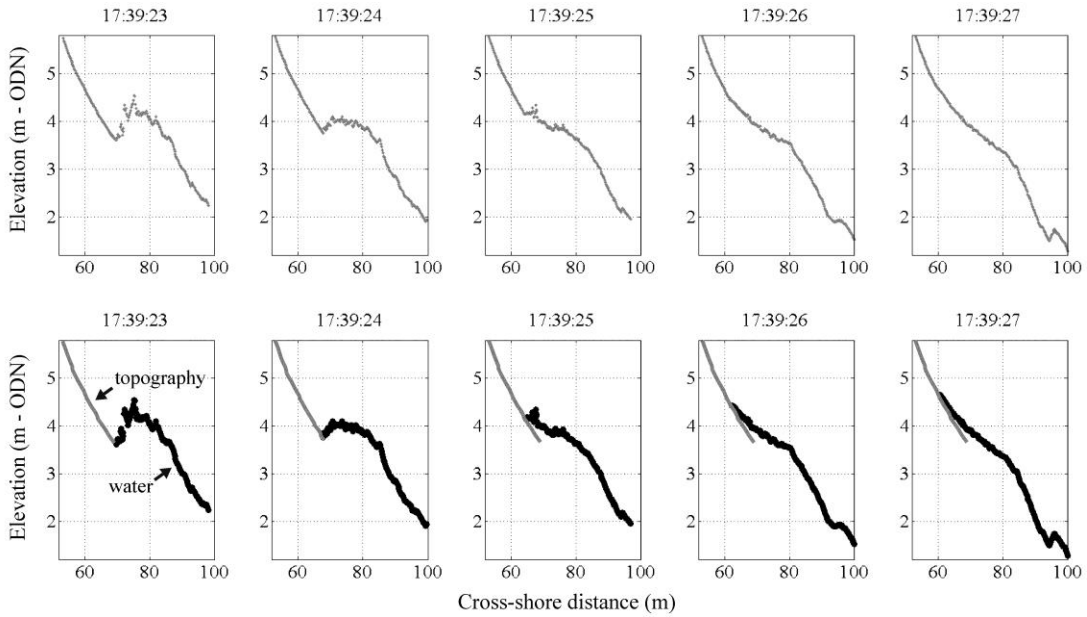

Fig. 6. Raw laser-scanner measurements without the separation between beach topography and water (top panels), and after applying the separation methods (lower panels).

3.4. Defining the separation threshold

Following Turner et al. (2008), a 40-min segment of laser measurements was analysed in order to perform an adequate selection of the variance threshold in Eq. (2) (Fig. 7). The selected data were obtained from a section of the beach profile landward of the swash zone and it can be assumed that no morphological change occurred over that period (Fig. 7). The variance was computed for segments of 4 s (Δt used in Eq. (2)) of measurements and for different angles of incidence of the laser beam within the selected section of the profile (Fig. 7). The results of this analysis indicate that for low angles of incidence (< 7°) the variance of the measurements increases significantly compared with the variance observed for large angles of incidence (> 7°). Based on these results two variance thresholds were defined: 6.6×10^{-4} m^2 for angles < 7°; and 2.2×10^{-4} m^2 for angles > 7°. These values are used in Eq. (2) to separate the stationary bed level from the non-stationary water surface. Because these thresholds are likely to depend on the nature of the bed material and the averaging interval, this procedure should be carried out for every deployment.

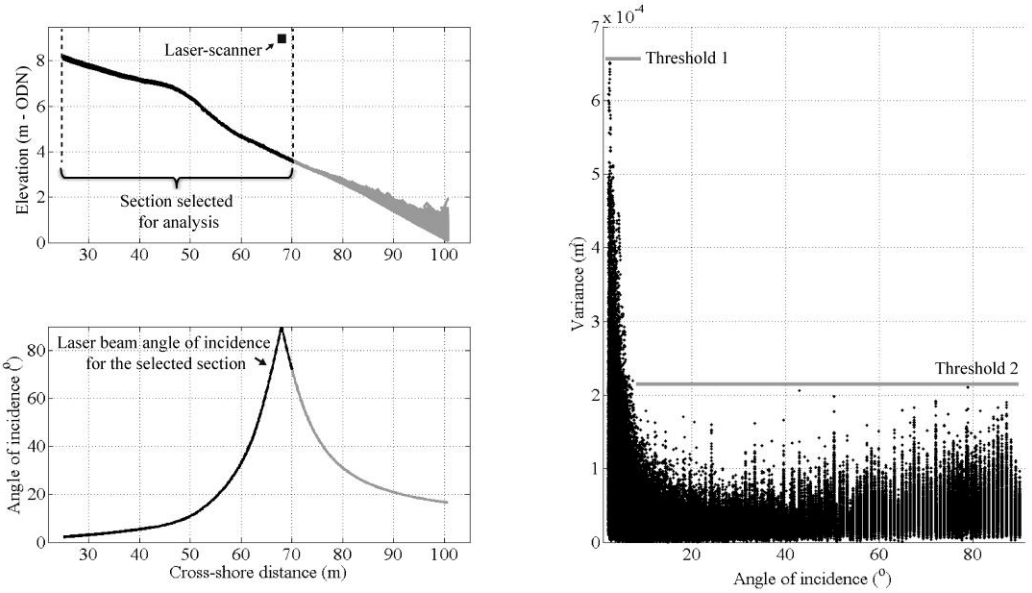

Fig. 7. Section of the beach profile analysed during 40 min of laser-scanner measurements and the respective angles of incidence (left panels); variance computed for each angle of incidence (right panel). The two horizontal lines in the right panel represent the two variance thresholds computed for two groups of angles of incidence.

3.5. Wave and tide records

Field measurements were obtained during a tide cycle at the peak of an energetic swell event (Fig. 8) on 24 March 2012. The offshore wave conditions observed at the peak of the event showed waves from the southwest with significant wave height (H_s) of 2.5 m and a peak period (T_p) of 12 s (Fig. 8). This event occurred during spring tides (tidal range of approximately 4 m) and the maximum offshore wave conditions occurred just after high tide (Fig. 8).

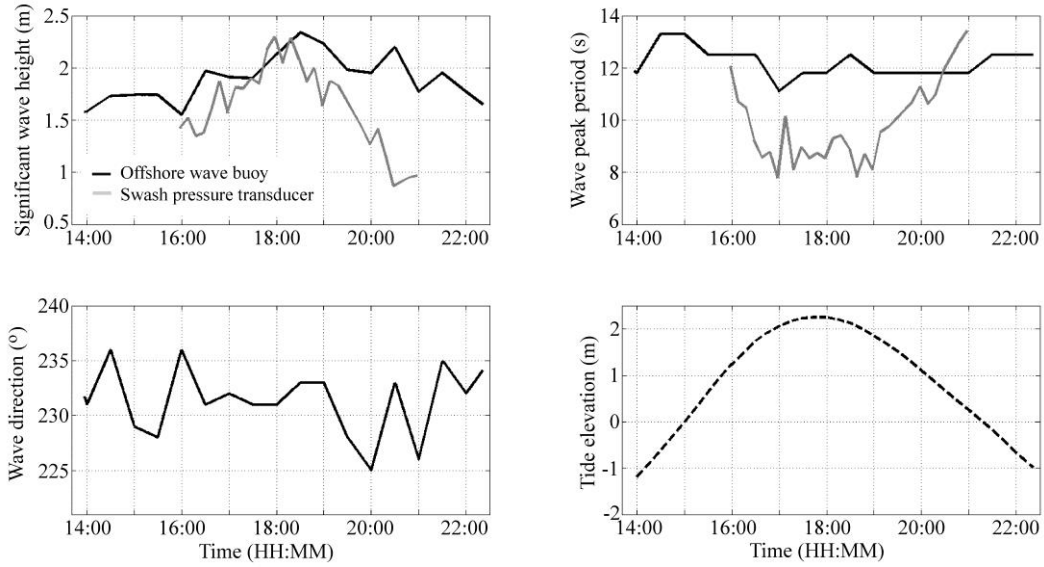

Fig. 8. Time series of significant wave height (upper left panel), peak wave period (upper right panel), wave direction (lower left panel) and tide elevation (lower right panel). Solid black lines represent offshore wave conditions measured by the offshore wave buoy, solid grey lines are measurements made by the pressure transducer on the beach deployed just above high tide level, and the dashed line represents tide measurements performed at Porthleven by a pressure transducer deployed around the MLWS level.

Also shown in Fig. 8 are comparative wave statistics measured in the swash zone obtained from the PT sensor deployed around the MLWS level. These show a strong tidal modulation of H_s and T_p relative to the offshore values. During mid-tide, the PT was in the mid to lower swash zone and mainly recorded large swash bores with the occasional breaking wave. The larger T_p values observed at this tidal stage are therefore due to the low-pass filtering effect that the breakpoint (Waddell, 1973) has on the offshore boundary of the swash. During high tide, the PT sensor was located at the transition of the lower swash and breakpoint, and recorded mostly breaking waves. Therefore, at this tidal stage every wave was recorded and H_s was larger and T_p shorter than the offshore measurements.

3.6. Data analysis

Swash hydrodynamics measured by the laser-scanner were analysed through the calculation of the following statistical parameters from the runup elevation time-series (R): (1) 2% exceedence of the runup maxima ($R_{2\%}$); (2) standard deviation of the vertical runup (R_σ); (3) runup vertical excursion (R_{exc}); (4) runup spectra; and (5) swash flow velocity skewness ($< u^3 >$) computed as:

$$\langle u^3 \rangle = \frac{\langle u^3 \rangle}{\langle u^2 \rangle^{1.5}} \qquad \text{(equation 3)}$$

where u is the cross-shore instantaneous velocity of the runup edge, computed through the first derivative of the runup elevation time series (Fig. 9). Wave dependence was removed from the first three runup parameters ($R_{2\%}$, R_σ and R_{exc}) by normalising by the significant offshore wave height.

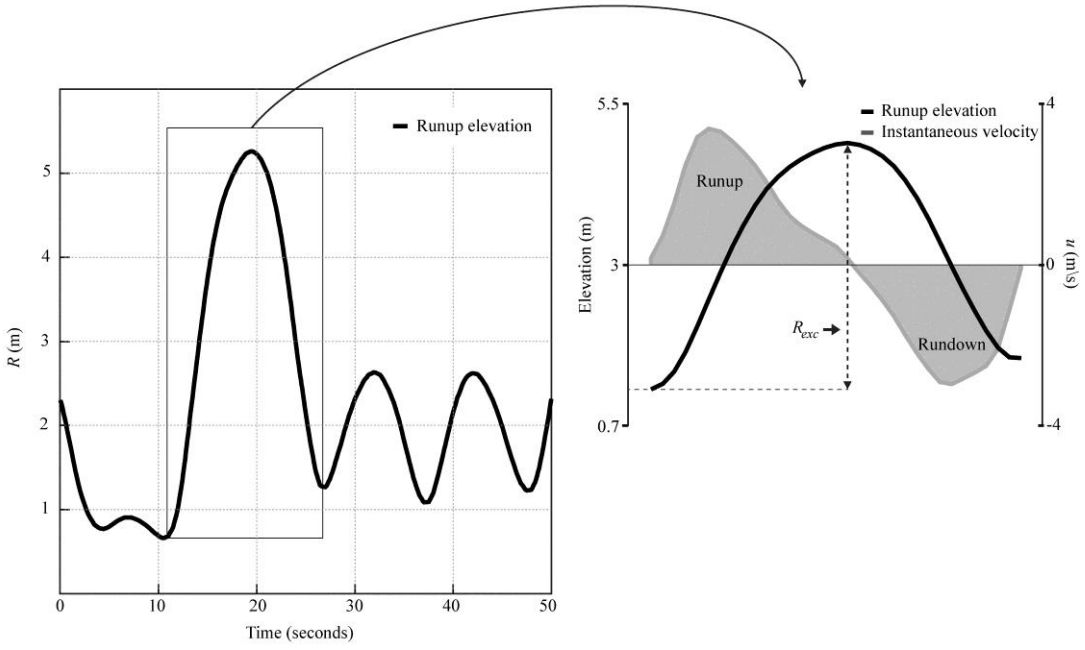

Fig. 9. Time series of runup elevation (R) and explanation for deriving swash instantaneous velocities (u) and vertical runup excursions (R_{exc}).

Swash morphological response was analysed by computing: (1) cumulative vertical difference between consecutive beach profiles measured with the laser-scanner; (2) beach gradient (slope of the region constrained by the upper runup and lower rundown limits); and (3) maximum elevation of the step deposit (maximum elevation of the deposition recorded in the lower swash zone). All hydrodynamic and morphological parameters were computed for continuous segments of 15 min of data.

3.7. Swash hydrodynamics

The complete *R* time series derived from the laser-scanner data includes 4 h at either side of high tide and is presented in Fig. 10. The *R* was obtained by corresponding the instantaneous shoreline (or the water's edge) to the cross-shore elevation at each time step. At first inspection, the runup motion during the rising tide appears less dynamic than that during the falling tide. This tidal asymmetry is explored further below using runup statistics computed over 15-min data segments (Fig. 11).

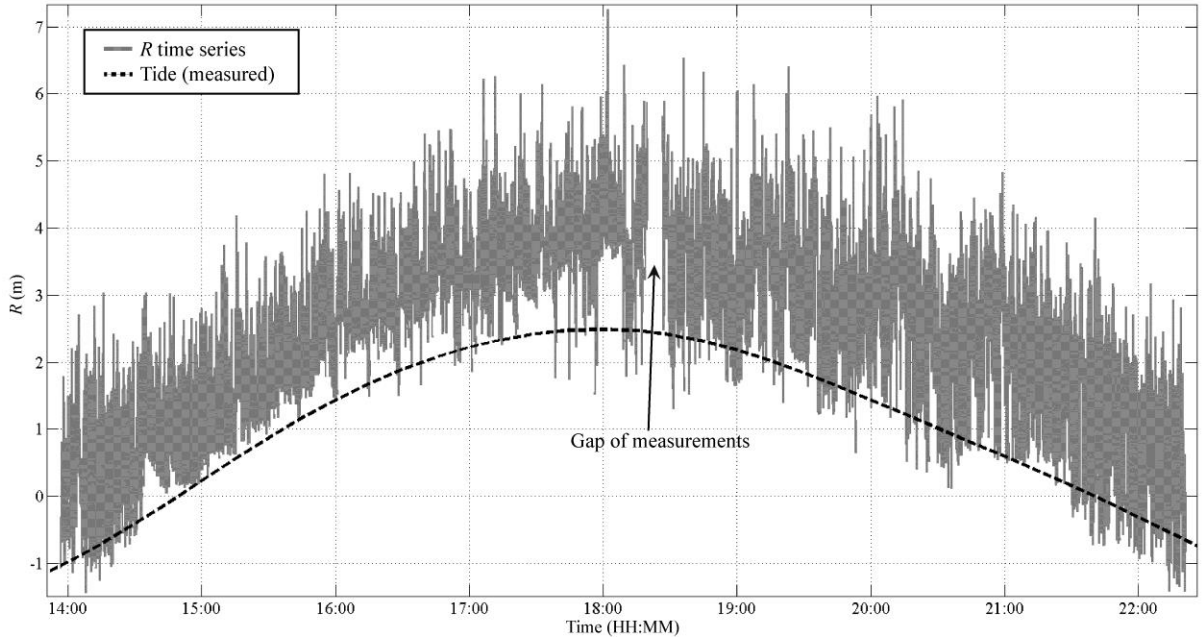

Fig. 10. Time series of runup elevation (*R*) measured by the laser-scanner (grey line) during one tidal cycle and the measured tide elevation (dashed black line).

The normalised 2% exceedence of the runup maxima ($R_{2\%}/H_s$) shows some variation over time not only with lower values (< 1.7) occurring between the mid rising and high tide (between 16:30 and 19:00) and higher values (> 2.1) mainly around the falling tide (between 19:00 and 22:30), but also with some peaks during the rising tide. The velocity skewness ($< u^3 >$), which is considered an indicator of the potential sediment transport direction, varied greatly during the entire tide cycle (Fig. 11). Strong runup dominance occurred during the initial rising tide phase (from 14:00 to 16:00), followed by 1.5 h of short periods of alternated flow direction dominance (first rundown and after runup). Between the high tide and 2 h after the beginning of the falling tide there was a strong rundown dominance, followed by another 2.5 h of alternated dominance.

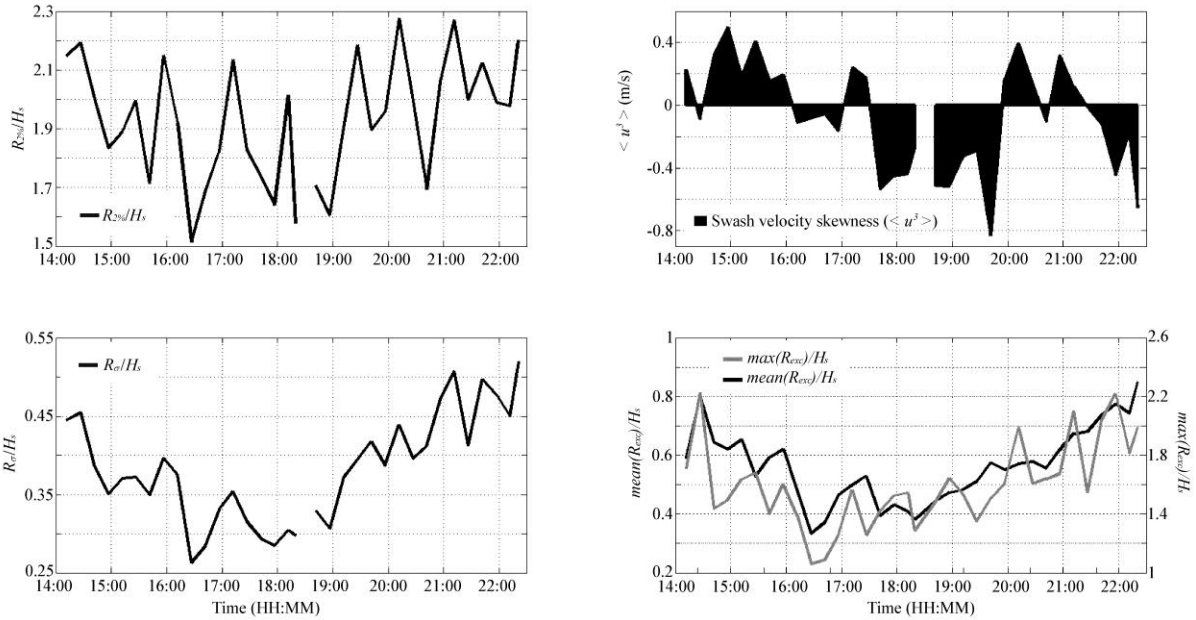

Fig. 11. Swash hydrodynamics calculated from the laser-scanner measurements: the normalised 2% exceedence of the runup maxima ($R_{2\%}/H_s$ — top left panel), swash velocity skewness ($< u^3 >$ — top right panel), normalised runup standard deviation (R_σ/H_s — bottom-left panel), and normalised mean and maximum runup vertical excursions ($mean(R_{exc})/H_s$ and $max(R_{exc})/H_s$ — bottom-right panel).

The normalised standard deviation of the runup elevation (R_σ/H_s) represents the runup energy and shows a gradual decrease over the rising tide and an increase over the falling tide (Fig. 11). The time series of the normalised mean and maximum runup vertical excursions ($mean(R_{exc})/H_s$ and $max(R_{exc})/H_s$ respectively) mirrors that of the runup standard deviation (Fig. 11).

Runup power spectra computed for 15 minute segments of R were averaged for the rising and falling tide phases (Fig. 12) and present two distinct peaks of energy at infragravity ($f < 0.05$ Hz) and incident ($f > 0.05$ Hz) frequencies during the two tidal phases. The peak around 0.08 Hz (12 s) on the incident band is in agreement with the offshore wave buoy and the inshore PT (Fig. 8), whilst a peak at 0.018 Hz (55 s) was found during both tidal phases in the runup spectra, which was not present in the offshore wave spectra (not shown). Runup spectra show that during the falling tide the amount of energy in the infragravity band is significantly higher than that during the rising tide, whilst the incident energy peak is smaller during the falling tide compared to the rising tide (Fig. 12). The significant runup elevation (S), computed for 15 minute segments of R following the method proposed by Stockdon et al. (2006), was normalised by the offshore H_s (S/H_s; Fig. 12) and shows a similar behaviour to the runup standard deviation and excursions, with lower values during the mid- and high-tide stages and higher values at the beginning of the rising and from mid- to low tide of the falling. The significant infragravity runup elevation (S_{ig}), computed for the $f < 0.05$ Hz band, is the dominant contributor to the total significant runup elevation (> 50%) during all the tidal stages (Fig. 12). The infragravity contribution is most important during mid- and high-tide stages, and less dominant during low tidal levels, although higher on the falling than during the rising tide.

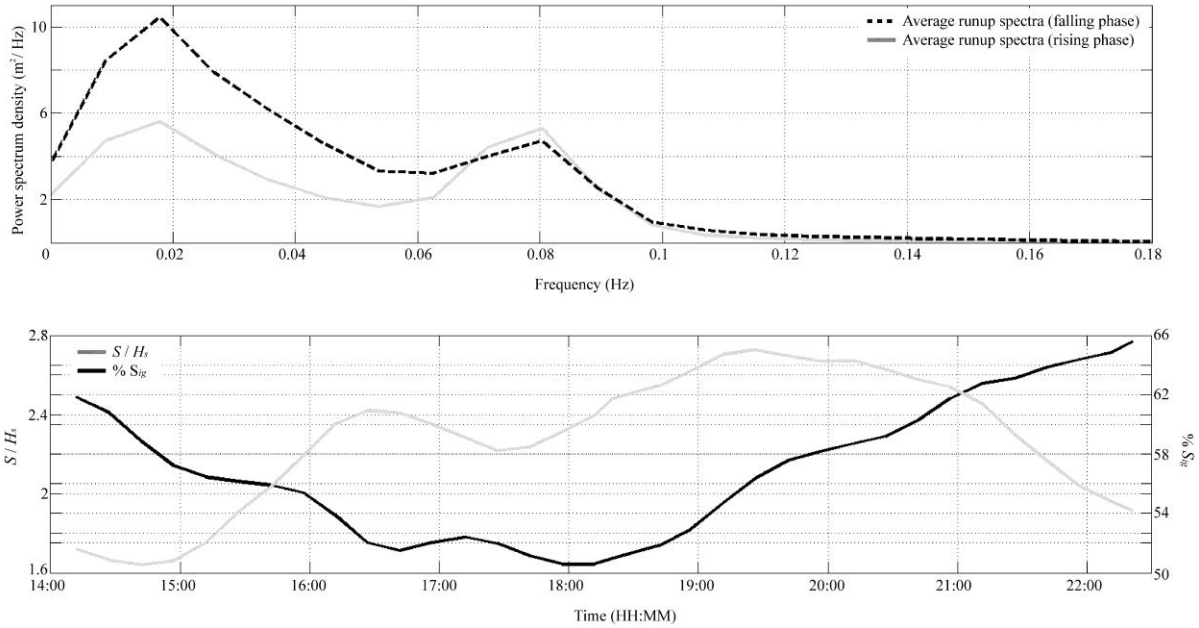

Fig. 12. Runup power spectra (top panel) averaged for the rising (grey line) and falling tide (dashed line). The spectra have 16 degrees of freedom and the frequency resolution is 0.0089 Hz. Significant normalised runup elevation (black line), normalised by the offshore significant wave height (S/H_s) and the percentage of the significant infragravity runup elevation ($\%S_{ig}$ — grey line) to the total runup energy (bottom panel).

3.8. Swash morphological response

Fig. 13 shows the morphological change over the recorded tide within the swash zone relative to the initial beach profile ('cumulative change') obtained from the laser scanner. The net morphological change over the tide was modest and characterised by c. 0.10 m accretion over most of the swash zone; however, the maximum cumulative change exceeded 0.6 m. The morphological response shows a distinct tidal asymmetry, with the rising tide being characterised by accretion on the lower beachface and erosion dominating the falling tide.

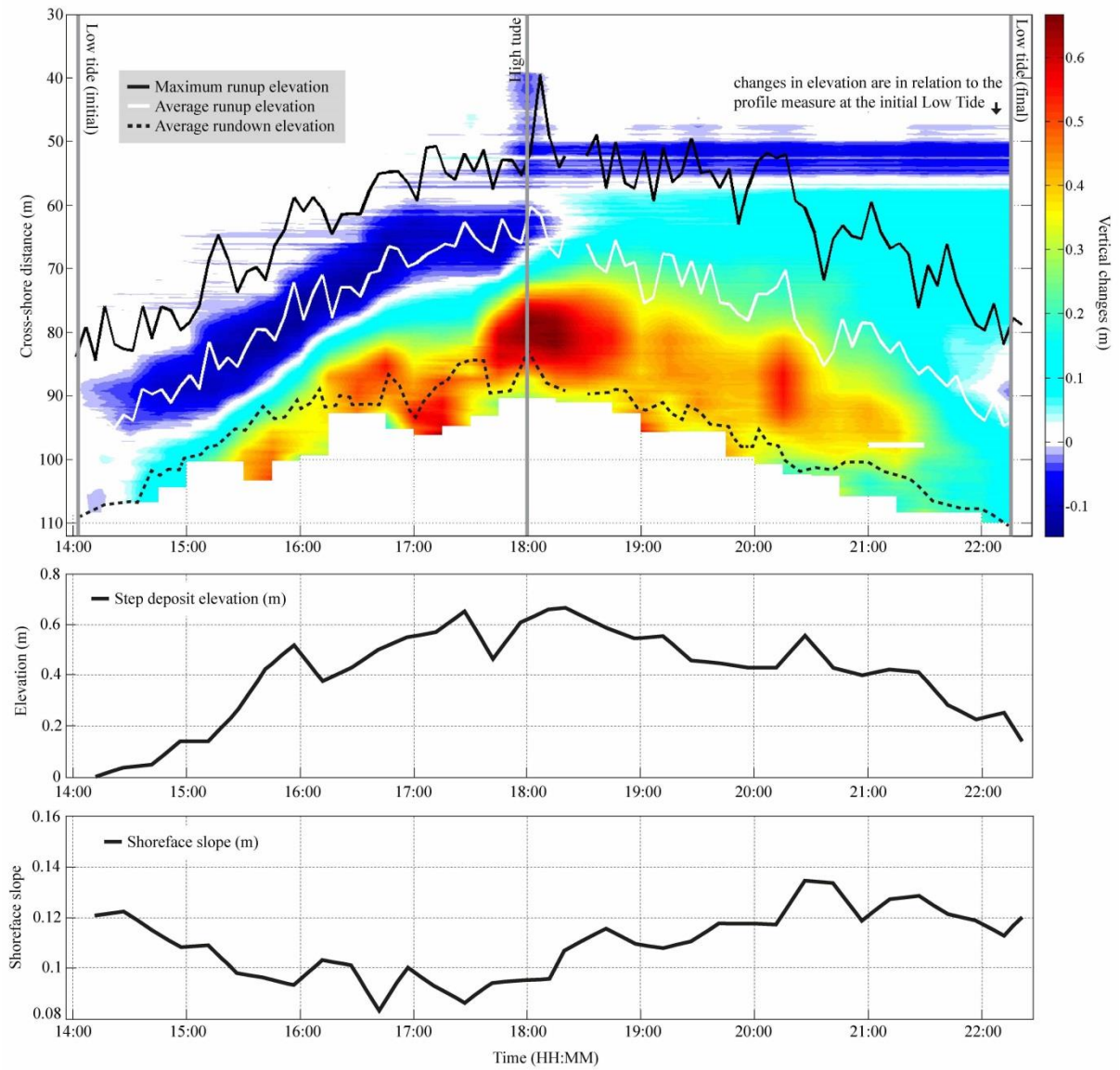

Fig. 13. Colour plot showing morphological change relative to the initial beach profile ('cumulative change') obtained from the laser-scanner during the tide cycle (top panel). The white and black lines represent the average and maximum runup elevations and the black dashed line represents the average rundown minima computed for consecutive segments of 15 min of measurements. Step deposit elevation (mid panel) and shoreface slope (lower panel) during the tide cycle.

During the initial stage of the rising tide (from 14:00 to 15:00) erosion occurred around the mid-swash zone (cross-shore distance = 90 m) and accretion took place over the lower swash zone (Fig. 13). This erosion/accretion pattern was sustained over the entire rising tide and by high tide (18:00) the deposit in the lower swash zone had attained its maximum thickness (c. 0.6 m). Because the sediment accumulation across the lower beachface significantly exceeded the amount of eroded material from the upper swash, it is likely that the source of this gravel was offshore and/or from alongshore transport. Field photos and visual observations indicate that the lower swash deposit was present along the entire beach, but was best developed within beach cusp troughs (Fig. 14).

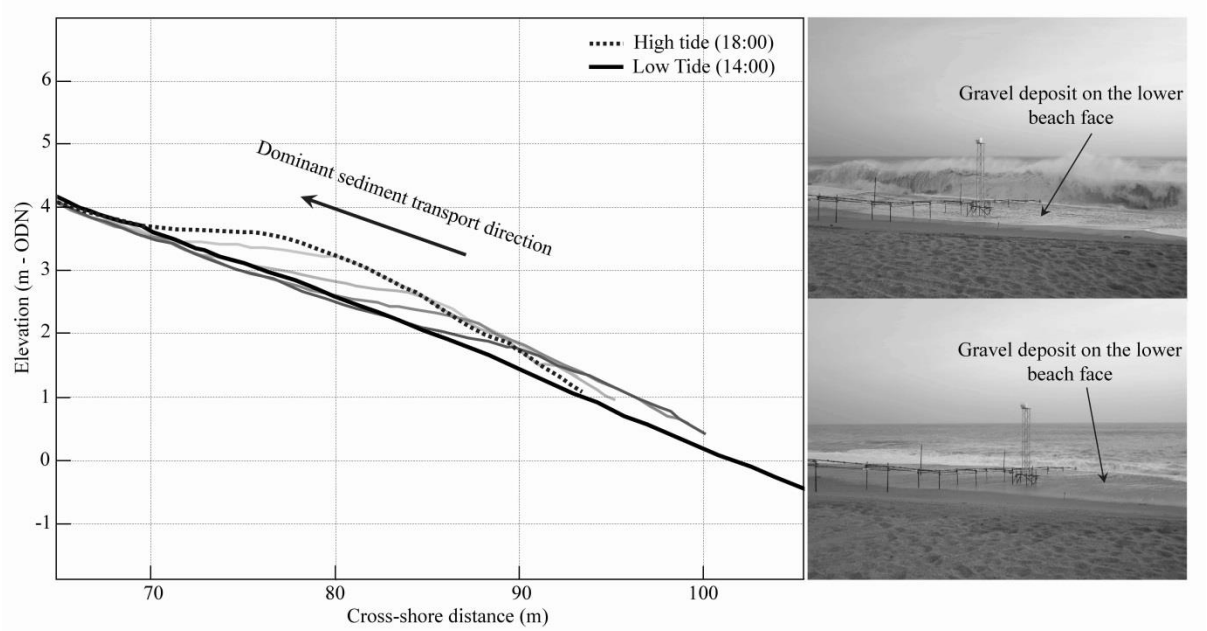

Fig. 14. Field photos taken at high tide showing the lower swash gravel deposit (right); several beach profiles showing several stages of growth of the lower beachface deposit during the rising tide phase (left).

The longshore consistency of this deposit during the rising tide phase provides strong evidence of a seaward source of this material (Fig. 14). Similar to underwater bedforms such as ripples, the shape of the deposit is characterised by a gentle up-current slope on the seaward face and a steeper slope on the landward face which suggests that the dominant flows were from seaward to landward, and the gravel was sourced from offshore.

At high tide the lower swash deposit reached its maximum vertical elevation (approximately 80 cm), but during the falling tide the feature progressively reduced in size. It appears that briefly after high tide, some of the material from the lower swash deposit is pushed onshore resulting in c. 0.1 m deposition in the upper swash region, but most of the sediment is taken offshore.

During the rising tide the average runup position correlates closely with the area of erosion in the upper swash zone (Fig. 13). During this stage of the tide, both the average and maximum runup positions follow the same trend with the same spacing between the two runup lines (c. 10 m). The rundown limit also follows the same trend until 16:00 when then it stabilizes and maintains approximately the same elevation until the high tide peak (18:00). At high tide there is a distinct drop in the average runup and rundown position; however, the maximum runup remains at the similar cross-shore position (at x = c. 55 m) until 19:30. During the falling tide both average and maximum runup and rundown positions decrease with a relatively constant spacing between the two lines (c. 15 m between average and maximum runup limits and 25 m between average runup and rundown limits), but the distance between the lines is significantly larger than that during the rising tide (Fig. 13).

An important consequence of these morphological changes observed on the swash zone is the flattening of the beachface. During the early stages of the rising tide, and until the peak of the high tide, the beachface slope reduces significantly (from 0.12 to 0.08; see Fig. 13). Initially (from 14:00 to 15:20) this occurs due to the erosion on the upper shoreface and accumulation on the lower part of the profile. Following this initial adjustment, the formation and development of the gravel deposit (from 15:30 until 18:00) significantly increases the elevation of the bed of the lower part of the profile, further decreasing the beachface slope (Fig. 13). At the peak of the high tide (around 18:00), the gravel deposit reached its maximum elevation (Fig. 13). After high tide, the shift in swash

hydrodynamics from onshore to offshore transport changes the sedimentation pattern and leads to the loss of sediment mainly towards the offshore. The significant lowering of the bed level across the lower shoreface increases the beachface gradient, which returns to its initial value (0.12; Fig. 13).

4. Discussion

The present paper describes the deployment of a 2D laser-scanner on a natural gravel beach to perform measurements of the morphology and hydrodynamics in the swash zone during an energetic wave event. The first part of the paper details the approach used to process the raw laser measurements, including a method to separate the beach topography from the water surface based on a variance threshold. The second part of the paper demonstrates the capabilities of the technique to investigate the swash morphodynamics during energetic conditions when in-situ instrumentation is unlikely to survive, let alone yield meaningful data.

4.1. Deployment and data analysis using a laser scanner

Only a few field experiments have used laser-scanner technology to perform similar types of measurements as that reported here (Blenkinsopp et al., 2010, Brodie et al., 2012 and Almeida et al., 2013), and, as a consequence, very little is known about specific aspects, such as behaviour of the laser measurements for different angles of incidence. The variability in the laser-scanner output was investigated for different angles of incidence during a period where no morphological changes occurred to provide insight into the vertical resolution of the data (Fig. 7). The results indicate that for angles lower than 7° the variance in the signal is larger than that for high angles of incidence. Taking into consideration that the reflecting angle of the laser beam is the same as the angle of incidence, there is a loss in energy and scanning range with decreasing incidence angle (SICK, 2009). This characteristic is important for data processing, since the proposed method for separating the raw measurements into bed level and water surface data is based on the identification of a variance threshold that defines the transition between stationary stages (e.g., detection of the bed) and non-stationary stages (e.g., vertical changes induced by the water motions). For the deployment described in this paper, this variance threshold for angles higher and lower than 7° was 1.5 cm and 3 cm, respectively, but this will depend on the type of scanner used and the beach sediments. The present deployment allowed complete coverage of the swash zone, spanning a cross-section of 90 m, and with an average horizontal resolution of 6 cm (Fig. 14).

4.2. Insight into gravel beachface morphodynamics gained using the laser scanner

The field measurements presented here describe the swash hydrodynamics and morphological response over a tidal cycle during energetic wave conditions on a gravel beach. The observations indicate that, despite the limited net morphological change over the tidal cycle, significant sediment mobilization occurred during the tide cycle. This result itself demonstrates the importance of being able to make high-frequency measurements on dynamic environments, such as gravel beaches. Such measurements would not be possible using conventional survey methods (e.g., low tide dGPS surveys). The morphological response recorded over an 8-hour period centred around high tide can be summarised by limited erosion in the upper swash zone and significant accretion in the lower swash zone during the rising tide, and limited accretion in the upper swash zone and significant erosion in the lower swash zone during the falling tide. A comprehensive interpretation of the laser-scanner measurements is presented in Fig. 15 and provides new insights into the morphodynamics of gravel beaches during energetic wave conditions ($H_s > 2$ m), whilst complementing previous similar

measurements made under mild wave conditions (H_s < 1 m; Kulkarni et al., 2004, Ivamy and Kench, 2006, Austin and Buscombe, 2008 and Masselink et al., 2010).

Stage 1

During the early stage of the rising tide, a sediment deposit forms in the lower swash zone, just above the still water level. The deposit is related to the development and onshore migration of the beach step, a relatively small and steep morphological feature at the base of the foreshore that forms a submerged break of slope at the base of the swash zone which appears to adjust to nearshore hydrodynamic regime (e.g., Hughes and Cowell, 1987). Advection of sediment entrained at the wave breaking point is the most likely mechanism (Voulgaris and Collins, 2000, Brocchini and Baldock, 2008 and Alsina et al., 2009) to explain the source of the accumulated material because the amount of eroded material from the upper swash is significantly less than the total amount accumulated on the lower swash. Since the contribution by longshore sediment transport processes is limited (the feature was present along the entire beach), the principal source of this material is considered to be the region just offshore of the step, as observed previously in field experiments with mild wave conditions (Strahler, 1966, Austin and Buscombe, 2008 and Masselink et al., 2010). It is suggested that the net onshore sediment transport within the swash zone is the combined result of positively-skewed runup flows (predominantly landward) and enhanced sediment suspension in the lower swash due to waves plunging directly onto the beachface whilst the step deposit is not very pronounced (cf. Masselink et al., 2010).

Stage 2

As the tide progresses and approaches high tide, the deposit in the lower swash zone continues to grow and migrate onshore, and the beach gradient in the swash zone decreases. This has a profound impact on the swash hydrodynamics through morphodynamic feedback not previously observed. Specifically, the swash dynamics become less energetic (as quantified by the decreasing trend in all runup parameters) and increasingly dominated by infragravity frequencies. The reason for this change in swash morphodynamics is that as the step feature continues to grow it becomes increasingly a focal point for wave breaking. In other words, the swash region is becoming a dissipative environment with the step feature protecting the mid- and upper swash zone from energetic swash action (Poate et al., 2013). The role of the step as an offshore energy dissipator, akin to that of nearshore bars on sandy beaches, has also been alluded to by several authors (Kulkarni et al., 2004, Buscombe and Masselink, 2006, Austin and Buscombe, 2008 and Masselink et al., 2010). Interestingly, during this stage of the tide, the skewness of the runup flows switches from positive to negative. By the end of this stage, at high tide, the deposit in the lower swash zone has reached its maximum thickness (0.6 m), the swash zone its minimum gradient (0.09) and the runup parameters (normalised by the offshore H_s) their minimum values; this indicates that the protective role of the step deposit is maximized at the high tide.

Stage 3

As soon as the tide begins to fall, onshore sediment transport in the swash zone and beachface accretion switch to offshore sediment transport and erosion. This stage is initially characterised by negatively-skewed flows (from 18:00 to 20:00) and in combination with relatively limited sediment suspension during the uprush (because waves dissipate their energy on the step feature) is suggested to be driving sediment offshore, resulting in erosion of the step deposit. A similar control of the step

on the swash zone sediment transport processes was also observed in gravel (Masselink et al., 2010) and mixed sand/gravel beach (Ivamy and Kench, 2006), during mild wave conditions. Another potentially important process contributing to offshore sediment transport in the swash zone during the falling tide is the change of the water table slope from landward to seaward, initiating groundwater seepage and promoting offshore sediment transport (Turner, 1990, Kulkarni et al., 2004 and Masselink and Turner, 2012). Erosion during the falling tide gradually removes the step deposit and leads to an increase in the beach gradient in the swash zone. In turn, this results in an increase in the (normalised) runup energy and a decrease in the importance of infragravity frequencies.

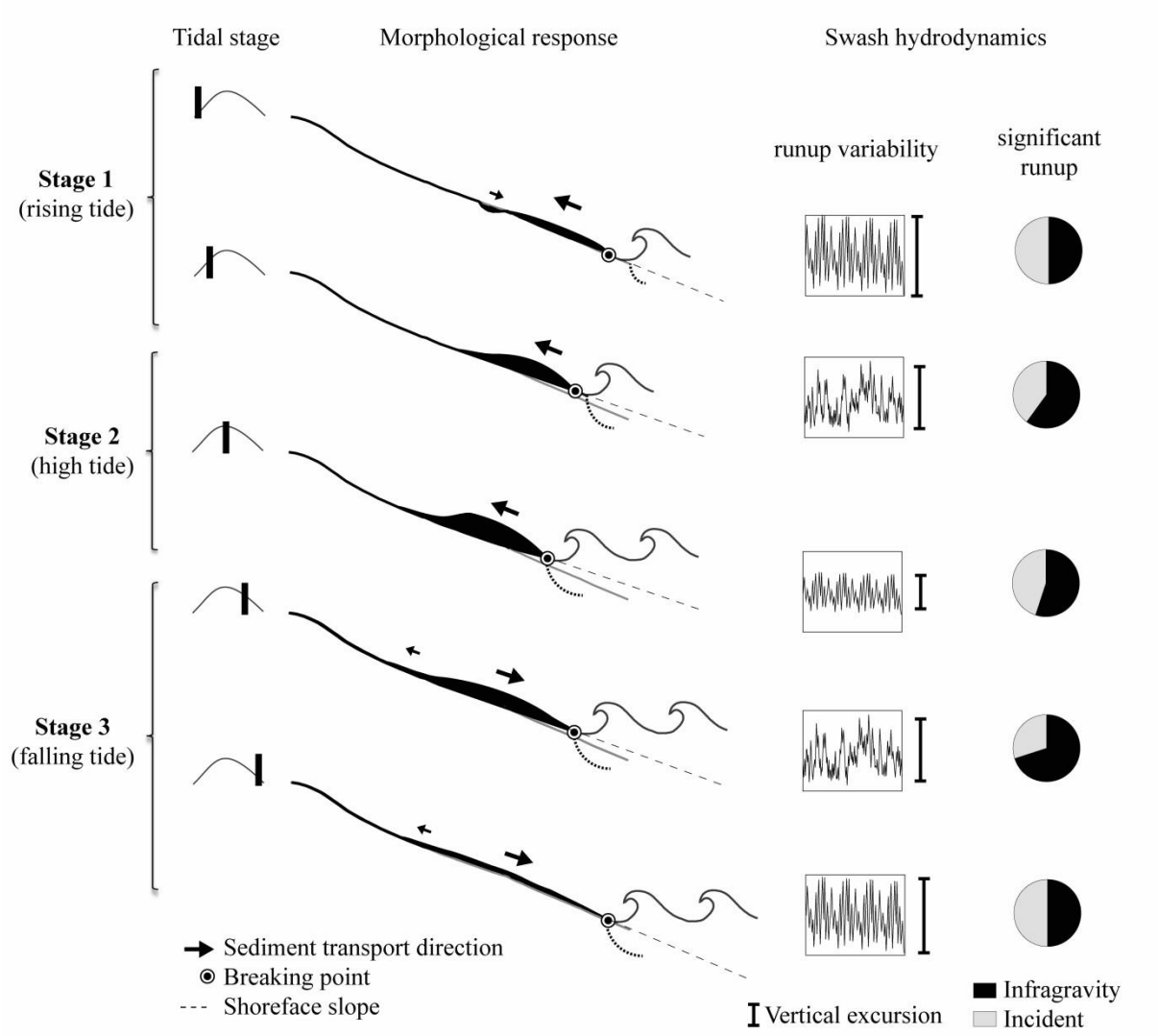

Fig. 15. Sketch of the morphological response and runup characteristics of a gravel beach, over a tidal cycle during energetic wave conditions.

The interpretation of the laser-scanner data synthesised in Fig. 15 is based on the assumption that the beachface morphology responds instantaneously to the hydrodynamic conditions (swash dynamics). However, it is important to recognise the existence of relaxation times and that it takes a finite amount of time for the morphology to adjust to the changing hydrodynamic conditions imposed by the tide. The tidal translation around mid-tide for the tidal cycle described in this paper represents a horizontal migration rate of 0.1 m per minute (6 m per hour). It is therefore not unlikely that the evolving step deposit (growing or shrinking) is at all time out of equilibrium with the swash and breaker conditions.

During the rising tide this means that the deposit is likely to be too low on the beach (lagging behind the rising tide), whilst during the falling tide it is likely to be too high on the beach (lagging behind the falling tide). It is not appropriate to speculate further on the potential implication of this process using the present dataset, but numerical modelling can be used to investigate the importance of relaxation time further. Future laser-scanner deployments on other beaches with different morphology and sedimentology, and varying forcing conditions should also provide further insights.

5. Conclusion

A 2D laser-scanner was deployed on a gravel beach to remotely measure high-frequency swash morphological change and hydrodynamics during an energetic wave event. This innovative method allowed the complete coverage of the swash zone with a vertical accuracy of approximately ± 1.5 cm and average horizontal resolution of 6 cm, during the entire tide cycle. Detailed analysis of the laser-scanner measurements provided new insights into the swash morphodynamics of gravel beaches during energetic wave conditions. Results indicate that despite the small net of morphological changes over the tide cycle, significant sediment mobilization occurred during the tide cycle. A clear asymmetrical morphological response was found during the different tidal phases: the rising tide is dominated by onshore sediment transport (accretionary phase) and the falling tide by offshore sediment transport (erosional phase). The main factor controlling this asymmetrical morphological response is the step migration that, depending on the tide phase, dictates the wave breaking point and consequently the amount of advected sediment provided to the uprush. The balance between the uprush and downrush decides the dominant direction of the swash sediment transport. During the rising tide the dominant accretion (step deposit development) decreases the shoreface slope and reduces the runup energy, whilst during the falling tide the dominant erosion (step deposit remobilization) increases the shoreface slope and increases the runup energy.

6. Acknowledgements

The work described in this publication was supported by the EPSRC project ARCoES — Adaptation and Resilience of the UK Energy System to Climate Change (EPSRC reference: EP/1035390/1) and by EPSRC grant EP/H040056/1 in partnership with the Channel Coastal Observatory (CCO), HR Wallingford and the Environment Agency. The authors of this work would like to thank the support provided by Peter Ganderton on the setup of the laser-scanner, and Robert McCall and Tim Poate for the field support during this experiment.

7. References

Almeida, L.P., Masselink, G., Russell, P., Davidson, M., Poate, T., McCall, R., Blenkinsopp, C., Turner, I.L., 2013. Observations of the swash zone on a gravel beach during a storm using a laser-scanner (Lidar). J. Coastal Res., 65, 636-641.

Alsina, J.M., Falchetti, S., Baldock, T.E., 2009. Measurements and modelling of the advection of suspended sediment in the swash zone by solitary waves. Coast. Eng., 56, 621–631.

Austin, M.J., Masselink, G., 2006. Observations of morphological change and sediment transport on a steep gravel beach. Mar. Geol., 229, 59–77.

Austin, M.J., Buscombe, D., 2008. Morphological change and sediment dynamics of the beach step on a macrotidal gravel beach. Mar. Geol., 249, 167–183.

Blenkinsopp, C.E., Turner, I.L., Allis, M.J., Peirson, W.L., Garden, L.E., 2012. Application of LiDAR technology for measurement of time-varying free-surface profiles in a laboratory wave flume. Coast. Eng., 68, 1-5.

Blenkinsopp, C.E., Turner, I.L., Masselink, G., Russell, P.E., 2011. Swash zone sediment fluxes: field observations. Coast. Eng., 58, 28-44.

Blenkinsopp, C.E., Mole, M.A., Turner, I.L., Peirson, W.L., 2010. Measurements of the time-varying free-surface profile across the swash zone obtained using an industrial lidar. Coast. Eng., 57, 1059-1065.

Brodie, K.L., Slocum, R.K., McNinch, J.E., 2012. New insights into the physical drivers of wave runup from a continuously operating terrestrial laser scanner. Final Proc. of Ocean's 12, Virginia, U.S.A., pp. 1-8.

Brocchini, M., Baldock, T.E., 2008. Recent advances in modeling swash zone dynamics: influence of surf–swash interaction on nearshore hydrodynamics and morphodynamics. Rev. Geophys., 46, RG3003.

Buscombe, D., Masselink, G., 2006. Concepts in gravel beach dynamics. Earth-Sci. Rev., 79, 33–52.

Holman, R. A., 1986. Extreme value statistics for wave run-up on a natural beach. Coast. Eng., 9, 527-544.

Horn, B.K., 1987. Closed-form solution of absolute orientation using unit quaternions. J. Opt. Soc. Am., 4, 629-642.

Hughes, M.G., Cowell, P.J., 1987. Adjustment of reflective beaches to waves. J. Coast. Res., 3, 153–167.

Ivamy, M.C., Kench, P.S., 2006. Hydrodynamics and morphological adjustment of a mixed sand and gravel beach, Torere, Bay of Plenty, New Zealand. Mar. Geol., 228, 137–152.

Jennings, R., Schulmeister, J., 2002. A field based classification scheme for gravel beaches. Mar. Geol., 186, 211-228.

Kulkarni, C.D., Levoy, F., Montfort, O., Miles, J., 2004. Morphological variations of a mixed sediment beachface (Teignmouth, UK). Cont. Shelf Res., 24, 1203–1218.

Lippmann, T.C., Holman, R.A., 1989. Quantification of sand bar morphology: a video technique based on wave dissipation. J. Geophys. Res., 94, 995–1011.

Matias, A., Williams, J.J., Masselink, G., Ferreira, Ó., 2012. Overwash threshold for gravel barriers. Coast. Eng., 63, 48–61.

Masselink, G, Turner, I.L., Conley, D.C., Ruessink, B.G., Matias, A., Thompson, C., Castelle, B., Wolters, G., 2013. BARDEX II: Bringing the beach to the laboratory – again!. J. Coastal Res., 65, 1545-1550.

Masselink, G., Turner, I.L., 2012. Large-scale laboratory investigation into the effect of varying back-barrier lagoon water levels on gravel beach morphology and swash zone sediment transport. Coast. Eng., 63, 23-38.

Masselink, G., Russell, P., Blenkinsopp, C.E., Turner, I.L., 2010. Swash zone sediment transport, step dynamics and morphological response on a gravel beach. Mar. Geol., 274, 50–68.

Masselink, G., Russell, P., Turner, I.L., Blenkinsopp, C., 2009. Net sediment transport and morphological change in the swash zone of a high-energy sandy beach from swash event to tidal cycle time scales. Mar. Geol., 267, 18-35.

Miettinen, M., Ohman, M., Visala, A., Forsman, P., 2007. Simultaneous localization and mapping for forest harvesters. Final Proc. of IEEE International Conference on Robotics and Automation, Rome, Italy, pp. 517-522.

Orford, J., Jennings, S.C., Pethick, J., 2003. Extreme storm effect on gravel-dominated barriers. Final Proc. of the International Conference on Coastal Sediments, St Petersburg, United States, pp. 1-12.

Pallejà, T., Teixidó M., Tresanchez, M., Palacín J., 2009. Measuring gait using a ground laser range sensor. Sensors, 9, 9133-9146.

Plant, N.G. and Holman, R.A., 1997. Intertidal Beach Profile Estimation Using Video Images. Mar. Geol., 140, 1–24.

Poate, T., Masselink, G., McCall, R., Russell, P., Davidson, M., Turner, I.L., 2013. Field measurements of gravel beach response during storm conditions. Mar. Geol., 342, 1-13.

Ruiz de Alegria-Arzaburu, A., Masselink, G., 2010. Storm response and beach rotation on a gravel beach, Slapton Sands, U.K. Mar. Geol., 278, 77–99.

SICK, 2009. LD-OEM1000 to 5100 Laser Measurement System – operating manual. SICK AG Waldkirch, Germany.

Strahler, A.N., 1966. Tidal cycle of changes in an equilibrium beach, Sandy Hook, New Jersey. J. Geol., 74, 247–268.

Stockdon, H.F., Holman, R.A, Howd, P.A. and Sallenger Jr., A. H., 2006. Empirical parameterization of setup, swash and runup. Coastal Eng., 53, 573–588.
Stockdon, H.F., Holman, R.A., 2000. Estimation of wave phase speed and nearshore bathymetry from video imagery. J. Geophys. Res., 105, 22015–22033.

Turner, I.L., Russell, P.E., Butt, T., 2008. Measurement of wave-by-wave bed-levels in the swash zone. Coastal Eng., 55, 1237–1242.

Turner, R.J., 1990. The effects of a mid-foreshore groundwater effluent zone on tidal-cycle sediment distribution in Puget Sound, Washington. J. Coastal Res., 6, 597-610.

Vásquez-Martín, R., Núnez, P., Bandera, A., Sandoval, F., 2009. Curvature-based environment description for robot navigation using laser range sensors. Sensors, 9, 5894-5918.

Voulgaris, G., Collins, M.B., 2000. Sediment resuspension on beaches: response to breaking waves. Mar. Geol., 167, 137–187.

Waddell, E., 1973. Dynamics of swash and implications to beach response. Technical Report 139, Coastal Studies Institute, Louisiana State University, Baton Rouge, U.S.A..

Williams, J.J., Buscombe, D., Masselink, G., Turner, I.L., Swinkels, C., 2012. Barrier dynamics experiment (BARDEX): Aims, design and procedures. Coast. Eng., 63, 3-12.